Implementation of Hybridly Protected Quantum Gates

Chunfeng Wu,[1,*] Chunfang Sun,[2] Gangcheng Wang,[2] Xun-Li Feng,[3] and X. X. Yi[2]

[1] *Science, Mathematics and Technology, Singapore University of Technology and Design, 8 Somapah Road, Singapore 487372, Singapore*

[2] *Center for Quantum Sciences and School of Physics, Northeast Normal University, Changchun 130024, China*

[3] *Department of Physics, Shanghai Normal University, Shanghai 200234, China*

(Received 19 March 2021; revised 25 August 2021; accepted 5 January 2022; published 1 March 2022)

We explore the implementation of hybridly protected quantum operations combining the merits of geometry and holonomy, dynamical decoupling approach, and dephasing-free feature based on a simple and experimentally achievable spin model. The implementation of the quantum operations can be achieved in different physical systems with controllable parameters. The protected quantum operations are hence controllable and well suited for resolving various quantum-computation tasks, such as executing quantum error-correction codes or quantum error mitigation. Our scheme is based on an experimentally achievable Hamiltonian with reduced requirement of computational resources and thus, it brings us closer towards realizing protected quantum operations for resolving quantum-computation tasks in near-term quantum devices.

DOI: 10.1103/PhysRevApplied.17.034003

I. INTRODUCTION

In recent years, quantum computation has demonstrated its super capabilities partially with state-of-the-art quantum technologies, however, we are still in the early stage of realizing full potential of quantum computation. Different types of errors in quantum-system evolution are one of the main issues hindering the further development of quantum computation. In principle, the errors could be detected and corrected by adding more qubits according to quantum error-correction codes (QECCs) [1–4]. Unfortunately, it is challenging to achieve required threshold values of errors with moderate computational resources in practical experiments, for realizing large-scale fault-tolerant quantum computation [4–6]. Thereafter, the theory of quantum error mitigation (QEM) was introduced to improve the accuracy of quantum algorithms with noisy intermediate-scale quantum devices [7,8], though the performance of the QEM also relies on the reliability of quantum operations at the level of physical qubits. It is therefore essential to achieve high-fidelity quantum operations for the development of quantum computation.

Various methods aiming to protect quantum operations have been investigated in the literature, such as geometric and holonomic quantum gates [9–14], dynamical decoupling (DD) approach [15–18] and the decoherence-free subspaces (DFSs) [19–21], etc. Quantum holonomy or geometric phase results in robust quantum operations insensitive to control imprecisions [9–14]. DD is one attractive approach to combat errors by using external controls to approximately average out undesired couplings with relatively modest resources [15–18]. DFSs provide efficient error-prevention schemes for fighting decoherence when system-environment interaction possesses certain symmetry since they are the subspaces invariant to nonunitary dynamics [19–21]. The preserved quantum operations by geometry and holonomy, and/or DFS, and/or DD are apparently useful in mitigating errors at the level of physical qubits, and hence have gained considerable attention in applying them in different quantum protocols, for example, protected QECCs [22–26]. By combining QECCs and the noise-resistant methods, it is expected the effect of errors can be further diminished without the need for a big increase in computational resource. The integration of QECCs and holonomic quantum operations has been explored in Refs. [22–26], but the integration of QECCs and multiple noise-resistant approaches is still open.

Actually there have been various schemes proposed for achieving robust quantum operations involving more than one of the noise-resistant methods, in order to mitigate the effects of multiple types of errors [27–31]. Specifically in Refs. [27–30], two noise-resistant methods are integrated and in Ref. [31], three methods are consolidated to achieve robust quantum operations. Nevertheless, the results in the literature are not effortlessly useful for implementing various quantum-computation tasks. Some of the reasons are discussed as follows. First, when combining

*chunfeng_wu@sutd.edu.sg

the different noise-resistant methods, only some specific quantum gate operations can be implemented and sometimes the gate operations may not be readily the gates required in different quantum algorithms. Multistep system evolution may be required to achieve the desired quantum operations involved in certain quantum algorithms and as a result, it is unknown whether the gate fidelities are sufficiently high without evaluation. Secondly, a large number of physical qubits are required due to the encoding of physical qubits in favor of the above mentioned noise-resistant approaches. For examples, three physical qubits are needed to form one computational qubit in Refs. [27–30]. Thirdly, some of the required system interactions for achieving the robust quantum operations are not easily realizable in physical systems with controllable parameters given a moderate resource of external drivings [27,28,30,31].

In this work, we explore the implementation of hybridly protected quantum operations based on one simple spin model, combining the merits of geometry and holonomy, DD approach, and dephasing-free feature. In the scheme, only two physical qubits are needed for encoding one computational qubit to support the noise-resistant approaches, reducing the requirement of computational resource. The simple spin model can be easily realized in different physical systems, and so can the hybridly protected quantum operations. We take a superconducting system as an example to explore the performance of the protected gates. With the robust quantum gates, it is possible to implement protected quantum algorithms, such as protected QECCs. Due to the noise-resistant properties offered by geometry and holonomy, DD and DFS, quantum operations are less sensitive to errors and therefore our scheme paves a promising way towards realizing fault-tolerant quantum tasks in near-term quantum devices.

II. QUANTUM GATES PROTECTED BY GEOMETRIC, HOLONOMIC AND DFS FEATURES

To achieve hybridly protected quantum gates, we consider the following interaction:

$$H=\sum_{m,n\neq m}\Omega_{mn}\left(\sigma_{+}^{m}\sigma_{-}^{n}+\sigma_{-}^{m}\sigma_{+}^{n}\right), \tag{1}$$

where Ω_{mn} describes the coupling strength between qubits m and n, and $\sigma_{\pm}^{m,n}=(1/2)(\sigma_{x}^{m,n}\pm i\sigma_{y}^{m,n})$. The type of interaction has been well explored in different physical systems with state-of-the-art experimental technologies, such as superconducting circuits [32–37] and trapped ions [38–40] with controllable system parameters. In most of the cases, the interaction can be readily achieved on neighbor pairs of physical qubits by applying or removing external drivings. In other words, the above desired interaction and hence the hybridly protected quantum operations discussed in the following are executable in different practical experiments.

A. Single-qubit gates with geometric and holonomic and dephasing-free merits

We first use three physical qubits to implement single-qubit protected quantum gates. Qubit A is the auxiliary qubit and the computational qubit is formed by qubits 1 and 2 in the following way $|0\rangle_L=|0\rangle_1|1\rangle_2$ and $|1\rangle_L=|1\rangle_1|0\rangle_2$, and therefore computational qubits are encoded in the DFS of dephasing. Given a system Hamiltonian by properly applying external drivings,

$$H_1=\Omega_{A1}\sigma_{+}^{A}\sigma_{-}^{1}+\Omega_{A2}\sigma_{+}^{A}\sigma_{-}^{2}+\text{h.c.}, \tag{2}$$

at $\tau_1=\pi/\Omega$ with $\Omega=\sqrt{\Omega_{A1}^2+\Omega_{A2}^2}$ and $\tan(\theta/2)=\Omega_{A1}/\Omega_{A2}$, we have an evolution operator from H_1,

$$U_1(\tau_1)=|0\rangle_A\langle 0|\otimes U_{1,0}(\tau_1)+|1\rangle_A\langle 1|\otimes U_{1,1}(\tau_1), \tag{3}$$

where $U_{1,m}(\tau_1)=(-1)^{m+1}\cos\theta\sigma_z^L-\sin\theta\sigma_x^L$ with $m=0,1$ written in the basis of $\{|0\rangle_L,|1\rangle_L\}$, where $\sigma_z^L=|0\rangle_L\langle 0|-|1\rangle_L\langle 1|$ and $\sigma_x^L=|0\rangle_L\langle 1|+|1\rangle_L\langle 0|$. The actual evolution operator from H_1 is in block-diagonal form in 8×8 space, and that is the reason we can consider $U_1(\tau_1)$ only in the subspace. If the auxiliary qubit is initially in its ground state $|1\rangle_A$, we obtain $U_{1,1}(\tau_1)$ acting on the computational qubit. We then define two subspaces $\mathcal{S}_0=\{|001\rangle,|010\rangle\}$ and $\mathcal{S}_1=\{|101\rangle,|110\rangle\}$ with the corresponding projection operators $P_{\mathcal{S}_0}=|001\rangle\langle 001|+|010\rangle\langle 010|$ and $P_{\mathcal{S}_1}=|101\rangle\langle 101|+|110\rangle\langle 110|$, to show the quantum holonomy possessed by $U_{1,1}(\tau_1)$. We first find $\mathcal{S}_m(\tau_1)=U_1(\tau_1)\mathcal{S}_m=\mathcal{S}_m$, and we observe $P_{\mathcal{S}_m}(t)H_1P_{\mathcal{S}_m}(t)=0$, where $P_{\mathcal{S}_m}(t)=U_1(t)P_{\mathcal{S}_m}U_1^{\dagger}(t)$. These results show that the two conditions for ensuring quantum holonomy are fulfilled [25]. Therefore, $U_{1,1}(\tau_1)$ is a holonomic matrix in the DFS of dephasing.

We then adjust system parameters to obtain the following Hamiltonian:

$$H_2=\Omega_{12}\sigma_{+}^{1}\sigma_{-}^{2}+\text{h.c.}, \tag{4}$$

and we find

$$\begin{aligned}U_2(\tau_2)&=e^{i\pi/(4\Omega_{12})H_2}U_1(\tau_1)U_1(\tau_1)\big|_{\theta=0}e^{-i\pi/(4\Omega_{12})H_2}\\&=|0\rangle_A\langle 0|\otimes U_{2,0}(\tau_2)+|1\rangle_A\langle 1|\otimes U_{2,1}(\tau_2),\end{aligned} \tag{5}$$

where $\tau_2=2\tau_1+\pi/(2\Omega_{12})$ and $U_{2,m}(\tau_2)=e^{i(-1)^m\theta\sigma_z^L}$. When the auxiliary qubit is in its ground state $|1\rangle_A$, we achieve single-qubit gates $U_{2,1}(\tau_2)$ acting on the computational qubit. From $U_{2,1}(\tau_2)$, we find that θ is the total

phase accumulated by the computational state $|m\rangle_L$ ($m = 0, 1$) and the phase is purely geometric. This is because the dynamic phase is zero from the investigation of the parallel transport condition (see Appendix A). Therefore, $U_{2,1}(\tau_2)$ describes single-qubit geometric gates acting on the computational qubit in the DFS of dephasing.

B. Two-qubit gates with geometric and holonomic and dephasing-free merits

For two-qubit protected quantum gates, we consider four physical qubits to form two computational qubits in the DFS of dephasing $\{|00\rangle_L, |01\rangle_L, |10\rangle_L, |11\rangle_L\}$, where $|00\rangle_L = |0\rangle_1 |1\rangle_2 |0\rangle_3 |1\rangle_4$, for example, and auxiliary qubits are not required. The system Hamiltonian is given by

$$H_3 = \Omega_{23}\sigma_+^2\sigma_-^3 + \Omega_{24}\sigma_+^2\sigma_-^4 + \text{h.c.} \tag{6}$$

We next control system parameters and get

$$H_4 = \Omega_{34}\sigma_+^3\sigma_-^4 + \text{h.c.} \tag{7}$$

Similarly through a four-step evolution according to H_3 and H_4, at $\tau_2' = 2\tau_1' + \pi/(2\Omega_{34})$, where $\tau_1' = \pi/\Omega'$ with $\Omega' = \sqrt{\Omega_{23}^2 + \Omega_{24}^2}$ and $\tan(\theta'/2) = \Omega_{23}/\Omega_{24}$, we find

$$\begin{aligned} U_4(\tau_2') &= e^{i\pi/(4\Omega_{34})H_4} U_3(\tau_1')U_3(\tau_1')\big|_{\theta'=0} e^{-i\pi/(4\Omega_{34})H_4} \\ &= e^{-i\theta'\sigma_z^L\otimes\sigma_z^L}, \end{aligned} \tag{8}$$

where $U_3(\tau_1')$ is the evolution operator from Hamiltonian H_3 at $t = \tau_1'$ written in the basis of $\{|00\rangle_L, |01\rangle_L, |10\rangle_L, |11\rangle_L\}$ (see Appendix A). It is clear that θ' is the total phase collected by state $|mn\rangle_L$ ($m, n = 0, 1$). The phase is entirely geometric since the dynamic phase is zero according to the parallel transport condition (see Appendix A). This shows $U_4(\tau_2')$ leads to two-qubit geometric gates acting on the two computational qubits.

III. DD FEATURE POSSESSED BY THE GATES

We show that a set of geometric and holonomic quantum gates acting in the DFS of dephasing can be implemented based on the interaction, Eq. (1). Special spotlight should be on another robust merit possessed by the quantum gates, and that is the feature of the applicable DD approach on the system evolution without causing noticeable disturbance. According to the DD approach, undesired couplings can be approximately averaged out by the decoupling group $\mathcal{G}$ that is usually selected as $\mathcal{G} = \{\mathbb{1}^{\otimes N}, \sigma_x^{\otimes N}, \sigma_y^{\otimes N}, \sigma_z^{\otimes N}\}$ for N physical qubits [41,42]. It is easy to show in our scheme that $[H_{1,2}, \mathcal{G}_j] = 0$ when $N = 3$ and $[H_{3,4}, \mathcal{G}_j] = 0$ when $N = 4$, where $\mathcal{G}_j$ is the jth element in $\mathcal{G}$ with $j = 1, \ldots, 4$. The results tell us that the resulting average system-bath coupling can roughly be reduced to nil with the decoupling group without noticeably affecting desired system interaction, and so the DD approach to mitigate decoherence effect is applicable in our scheme of executing geometric and holonomic quantum gates in the DFS of dephasing. We later take periodic DD (PDD) as an example to demonstrate the protection offered by the DD approach in our scheme. Therefore, we are able to implement a set of hybridly protected quantum gates, combining the merits of geometry and holonomy, DD and DFS based on the simple and experimentally achievable interaction.

IV. PERFORMANCE OF THE PROTECTED GATES

In the following, we investigate the implementation of the hybridly protected quantum gates in superconducting circuits.

A. Protected gates in the absence of errors or noises

The system consists of an array of quantum Rabi models (QRMs), in which each QRM is just one effective qubit and the coupling between effective qubits is by controllable hopping interaction via a superconducting quantum interference device (SQUID) [43], as demonstrated in Fig. 1.

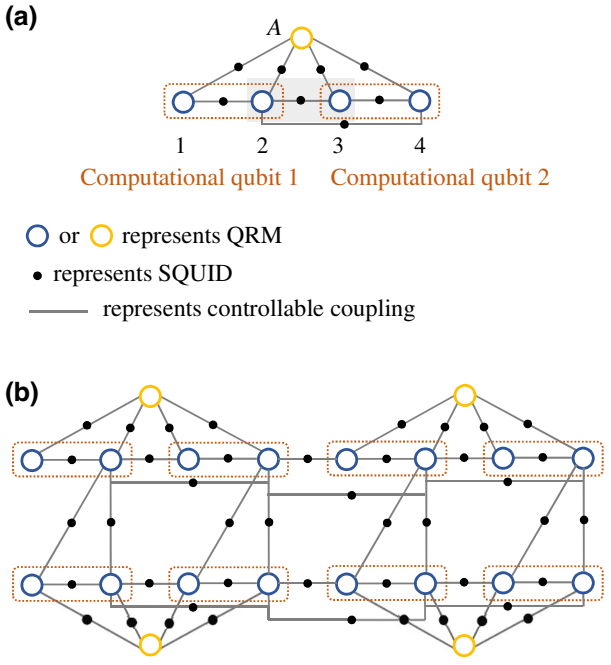

FIG. 1. Schematic setup of tunably coupled QRMs through SQUIDs. (a) Two computational qubits are formed by four QRMs, and QRM A is the auxiliary qubit to realize the single-qubit gate on computational qubit 1 or 2. (b) Generalization to a two-dimensional lattice of QRMs.

The system Hamiltonian of three-neighbor QRMs is [43]

$$H_{c\mathrm{QRM}} = \sum_{m=1}^{3} H_m^r + J_{12}\cos(\omega_{12}t+\phi_{12})(a_1^\dagger+a_1)(a_2^\dagger+a_2) + J_{13}\cos(\omega_{13}t+\phi_{13})(a_1^\dagger+a_1)(a_3^\dagger+a_3), \quad (9)$$

where $H_m^r = \omega_m^c a_m^\dagger a_m + (\omega_m^q/2)\sigma_{z,m} + g_m(a_m^\dagger + a_m)\sigma_{x,m}$ (ω_m^c, ω_m^q, and g_m represent resonator frequency, physical qubit frequency, and qubit-resonator coupling strength, respectively) is the Hamiltonian of mth QRM, and J_{mn}, ω_{mn}, and ϕ_{mn} describe the coupling strength, frequency, and phase of the hopping interaction [43]. As illustrated in Appendix B, $H_{c\mathrm{QRM}}$ in the interaction picture with respect to $\sum_{m=1}^{3} H_m^r$ almost ideally brings us the interaction described by Eq. (1) with $\sigma_\pm^m$ replaced by Pauli operations acting on effective qubits [43]. Specifically, several numbers of lowest energy levels of QRMs are considered and, as explained in Appendix B, the coupled QRMs can be described by coupled effective qubits with more higher-energy levels presented by properly selecting system parameters. The two desired effective Hamiltonians for realizing different protected single- and two-qubit quantum gates can be derived with only one [for Hamiltonian (4)] or two [for Hamiltonian (2)] external drivings, reducing the need for more resource of external drivings. In the superconducting system, we evaluate the performance of our scheme by randomly selecting 30 initial states for each gate. Moreover, the following parameters are selected: $\omega_m^c = 2\pi \times 7$ GHz, $\omega_m^q = 2\pi \times 6.1$, or 5.1 GHz, $g_m = 2\pi \times 2$ GHz, $\Omega = \Omega' = 2\pi \times 2$ MHz, which determine the values of J_{mn}, see details in Appendix B. In the following calculations without and with errors or noises, we choose only two lowest energy levels of each QRM to reduce the difficulty of numerically managing a large Hilbert space. The fidelities of various single- and two-qubit gates are demonstrated in Tables I, II, and III. In the absence of errors or noises, we obtain excellent gate fidelities.

TABLE II. Realization of a universal set of quantum gates in the system of coupled QRMs without or with dephasing effect, where DP is short for dephasing.

Gate	Realization	F without DP	F with DP
σ_x^L	$-U_{1,1}(\tau_1)\big\|_{\theta=\pi/2}$	$\approx 0.9999+$	≈ 0.9948
σ_z^L	$U_{1,1}(\tau_1)\big\|_{\theta=0}$	$\approx 0.9999+$	≈ 0.9948
H^L	$U_{1,1}(\tau_1)\big\|_{\theta=-\pi/4}$	$\approx 0.9999+$	≈ 0.9953
S^L	$e^{i\frac{\pi}{4}}U_{2,1}(\tau_2)\big\|_{\theta=\pi/4}$	$\approx 0.9999+$	≈ 0.9748
T^L	$e^{i\frac{\pi}{8}}U_{2,1}(\tau_2)\big\|_{\theta=\pi/8}$	$\approx 0.9999+$	≈ 0.9762
$e^{i\frac{\pi}{4}\sigma_z^L\otimes\sigma_z^L}$	$U_4(\tau_2')\big\|_{\theta'=-\pi/4}$	$\approx 0.9999+$	≈ 0.9531
CZ^L	$e^{-i\frac{\pi}{4}}(S^L\otimes S^L)$ $U_4(\tau_2')\big\|_{\theta'=-\pi/4}$	$\approx 0.9999+$	≈ 0.9057

B. Protection by geometric or holonomic feature

It is reasonable to expect lower gate fidelities when decoherence or noise effects are considered. Fortunately, some of the negative effects can be passively protected by the geometric or holonomic feature since it is insensitive to some control imprecision, as explained in the literature. Taking holonomic feature as an example, the system evolution over $[0, t_0]$ is governed by [12,25]

$$U(t_0) = Te^{-i\int_0^{t_0}[G(t)+D(t)]dt}, \quad (10)$$

where $G(t)$ and $D(t)$ are, respectively, due to geometric and dynamical effects with elements given by

$$G_{jk}(t) = -i\langle\psi_j(t)|\,|\dot{\psi}_k(t)\rangle, \quad D_{jk}(t) = \langle\psi_j(t)|\,H\,|\psi_k(t)\rangle, \quad (11)$$

where $|\psi_k(t)\rangle$ describes a basis of the subspace in which holonomic gates are implemented. In the presence of specific control imprecision, H may be changed to H^e but meanwhile the cyclic evolution condition is still fulfilled at desired time. This change does not affect the geometric term, and leads to

$$D_{jk}^e(t) = \langle\psi_j(t)|\,H^e\,|\psi_k(t)\rangle. \quad (12)$$

TABLE I. Realization of a universal set of quantum gates [where $S^L = \mathrm{diag}(1,i)$ and $T^L = \mathrm{diag}(1, e^{i\frac{\pi}{4}})$] in the system of coupled QRMs without or with control errors.

Gate	Realization	F without errors	$1-F$ without errors	F with errors	$1-F$ with errors
σ_x^L	$-U_{1,1}(\tau_1)\big\|_{\theta=\pi/2}$	$\approx 0.9999+$	$\approx 1.36\times10^{-6}$	$\approx 0.9999+$	$\approx 1.37\times10^{-6}$
σ_z^L	$U_{1,1}(\tau_1)\big\|_{\theta=0}$	$\approx 0.9999+$	$\approx 8.14\times10^{-7}$	$\approx 0.9999+$	$\approx 7.66\times10^{-7}$
H^L	$U_{1,1}(\tau_1)\big\|_{\theta=-\pi/4}$	$\approx 0.9999+$	$\approx 5.18\times10^{-7}$	$\approx 0.9999+$	$\approx 5.33\times10^{-7}$
S^L	$e^{i\frac{\pi}{4}}U_{2,1}(\tau_2)\big\|_{\theta=\pi/4}$	$\approx 0.9999+$	$\approx 9.84\times10^{-6}$	$\approx 0.9999+$	$\approx 9.99\times10^{-6}$
T^L	$e^{i\frac{\pi}{8}}U_{2,1}(\tau_2)\big\|_{\theta=\pi/8}$	$\approx 0.9999+$	$\approx 1.41\times10^{-5}$	$\approx 0.9999+$	$\approx 1.40\times10^{-5}$
$e^{i\frac{\pi}{4}\sigma_z^L\otimes\sigma_z^L}$	$U_4(\tau_2')\big\|_{\theta'=-\pi/4}$	$\approx 0.9999+$	$\approx 1.28\times10^{-5}$	$\approx 0.9999+$	$\approx 1.30\times10^{-5}$
CZ^L	$e^{-i\frac{\pi}{4}}(S^L\otimes S^L)U_4(\tau_2')\big\|_{\theta'=-\pi/4}$	$\approx 0.9999+$	$\approx 3.24\times10^{-5}$	$\approx 0.9999+$	$\approx 3.29\times10^{-5}$

TABLE III. Realization of a universal set of quantum gates in the system of coupled QRMs without or with different types of decoherences. When considering decoherences, the system-environment coupling includes the elements in x, y, and z directions and its magnitude is selected to be one tenth of Ω (see Appendix C). The fidelities in the presence of decoherences can be further improved by increasing the number of times of repeating the base sequence of PDD.

		Without decoherences	With decoherences	
Gate	Realization	Fidelity	Fidelity without DD	Fidelity with PDD repeated ten times
σ_x^L	$-U_{1,1}(\tau_1)\big\|_{\theta=\pi/2}$	$\approx 0.9999+$	≈ 0.7148	≈ 0.9975
σ_z^L	$U_{1,1}(\tau_1)\big\|_{\theta=0}$	$\approx 0.9999+$	≈ 0.7435	≈ 0.9982
H^L	$U_{1,1}(\tau_1)\big\|_{\theta=-\pi/4}$	$\approx 0.9999+$	≈ 0.6736	≈ 0.9987
$S^L=\mathrm{diag}(1,i)$	$e^{i\frac{\pi}{4}}U_{2,1}(\tau_2)\big\|_{\theta=\pi/4}$	$\approx 0.9999+$	≈ 0.1265	≈ 0.9898
$T^L=\mathrm{diag}(1,e^{i\frac{\pi}{4}})$	$e^{i\frac{\pi}{8}}U_{2,1}(\tau_2)\big\|_{\theta=\pi/8}$	$\approx 0.9999+$	≈ 0.1234	≈ 0.9897
$e^{i\frac{\pi}{4}\sigma_z^L\otimes\sigma_z^L}$	$U_4(\tau_2')\big\|_{\theta'=-\pi/4}$	$\approx 0.9999+$	≈ 0.0935	≈ 0.9841
CZ^L	$e^{-i\frac{\pi}{4}}(S^L\otimes S^L)U_4(\tau_2')\big\|_{\theta'=-\pi/4}$	$\approx 0.9999+$	≈ 0.0015	≈ 0.9641

If H^e is so special that $D_{jk}^e(t)=0$, we can say the resultant quantum gate is robust to the specific control imprecision due to the holonomic feature. While if the dynamical part $D_{jk}^e(t)$ is nonzero, it may be different from $D_{jk}(t)$ and so the resultant quantum gate is not robust.

It has been shown in Ref. [25] that holonomic gates are robust against stochastic fluctuations. We similarly show the robustness of our gates by considering the stochastic errors in H_j $(j=1,2,3,4)$. Specifically, we write

$$H_1^e=\Omega_{A1}^e\sigma_+^A\sigma_-^1+\Omega_{A2}^e\sigma_+^A\sigma_-^2+\mathrm{h.c.}, \tag{13}$$

where $\Omega_{Aj}^e=\Omega_{Aj}+\delta\Omega_{Aj}$ indicates the errors fluctuating around Ω_{Aj}, described by the Gaussian distribution with a standard deviation of $0.1\Omega_{Aj}$. In the case that the cyclic condition is fulfilled with the errors, $U_1(\tau_1)$ is robust against the control errors since dynamical part is zero. In similar ways, we assume the errors in $H_{2,3,4}^e$. The numerical results are summarized in Table I. Given the stochastic fluctuations in system parameters, the performance of the holonomic or geometric gates are not noticeably affected. The fidelities without and with errors are not the same, but with very small differences. The insignificant differences are due to numerical reasons, including slight changes in the evolution equation with stochastic fluctuations and finite number of steps in solving the evolution equation, which affects the selected number of stochastic fluctuations.

C. Protection by dephasing-free feature

When the system-environment interaction possesses some symmetry, the decoherences can be passively protected by the DFS approach. In our scheme, computational qubits are formed in the dephasing-free subspace. Namely with the dephasing

$$|0\rangle_m\to|0\rangle_m \quad\text{and}\quad |1\rangle_m\to e^{i\varphi}|1\rangle_m, \tag{14}$$

where φ is a random phase, $|\psi\rangle_L=a|0\rangle_L+b|1\rangle_L$ remains invariant under the dephasing, up to φ, which is a global phase. But the encoding in our scheme provides only passive protection against the dephasing with the symmetry. Passive protection demonstrates that the DFS approach is not helpful if the quantum system is deviated from the DFS due to uncontrollable effects.

In this subsection, we investigate the passive protection in the system of coupled QRMs through the following master equation [44]:

$$\dot\rho=-i[H_s,\rho]+\sum_k\gamma_z\mathcal{D}[\tilde\sigma_z^k]\rho, \tag{15}$$

where $\mathcal{D}[\tilde\sigma_z^k]\rho=\tilde\sigma_z^k\rho(\tilde\sigma_z^k)^\dagger-(1/2)(\tilde\sigma_z^k)^\dagger\tilde\sigma_z^k\rho-(1/2)\rho(\tilde\sigma_z^k)^\dagger\tilde\sigma_z^k$, $\tilde\sigma_z^k=|\tilde0_k\rangle\langle\tilde0_k|-|\tilde1_k\rangle\langle\tilde1_k|$ with $|\tilde0_k\rangle$ and $|\tilde1_k\rangle$ describing the two lowest states of the kth QRM, $\gamma_z=\sum_{j=1}^5\gamma_0|s_{00}^j-s_{11}^j|^2/4$, and $s_{nn}^j=\langle\tilde n|S^j|\tilde n\rangle$ $(n=0,1)$ with S^j being the elements in $S=\{\sigma_x,\sigma_y,\sigma_z,a+a^\dagger,i(a-a^\dagger)\}$ [44].

Since we use the Hamiltonians with applying the rotating-wave approximation in our numerical calculations, the Hamiltonians are slightly different from the effective ones. As a result, the system will evolve out of the dephasing-free subspace partially over time due to the effect of the terms neglected according to the rotating-wave approximation. The more the evolution time, the worse the protection provided by the DFS feature is. Here we choose $\gamma_0=2\pi\times10$ kHz, and list out the fidelities for single- and two-qubit gates without and with dephasing in Table II. The passive protection by the dephasing-free feature is clearly illustrated from the numerical results. For $U_{2,1}$ and U_4, we obtain worse fidelities than those for $U_{1,1}$ since there are four steps of evolution to achieve $U_{2,1}$ or U_4, while only one step of evolution to achieve $U_{1,1}$. The gate fidelities will become poorer and poorer with increasing dephasing rate, and this is because the

errors will be accumulated faster over time given higher dephasing rate.

D. Protection by DD feature

Fortunately in our scheme, different decoherences can be actively mitigated via the DD approach since our effective Hamiltonians commute with the decoupling group, regardless of the symmetry possessed by system-environment interaction. We explore the protection offered by the DD approach in the following and illustrate the active protection offered through diligently averaging decoherences out. To realize the DD approach, the decoupling group elements should be described by the Pauli operations acting on the effective qubits or QRMs. It is shown in Ref. [43], single-effective-qubit operations and thus the Pauli operations can be executed by applying external drivings on physical qubits. In Table III, we also present the fidelity for different gates in the presence of decoherences caused by system-environment interaction in all x, y, and z directions, when the DD approach is applied or not (see Appendix C). The DD approach used in our calculations is the PDD with repeated pulse sequences [16,18], while other DD techniques involving the decoupling group elements are applicable as well. By repeating a base pulse sequence $Z[\cdot]X[\cdot]Z[\cdot]X[\cdot]$ ten times (where Z and X indicate the global Pauli operators acting on the effective qubits, formed by the decoupling group elements), we get excellent gate fidelities even with the decoherences in all x, y, and z directions when the system-environment coupling strength is one tenth of that of the coupling between effective qubits, see Table III. The fidelities for the gates based on $U_{2,1}$ and U_4 are not as good as those for the gates based on $U_{1,1}$. This is because the system needs to undergo four-step evolution to achieve $U_{2,1}$ or U_4, while only one-step evolution to achieve $U_{1,1}$. Further improvements in gate fidelities can be achieved by increasing the number of times of repeating the base pulse sequence.

V. PROTECTED GATES AND POSSIBLE APPLICATIONS

We investigate the implementation of the protected quantum gates in the superconducting circuits, both Clifford and non-Clifford gates. It is well known that Clifford gates alone are not universal, but together with a non-Clifford T gate, any quantum operations can be generated. Therefore, the set of protected quantum gates can achieve a universal set of quantum gates for quantum computation, leading to various applications in resolving quantum-computation tasks. We then discuss the use of the protected quantum operations in QECCs by considering surface codes as an example. It is generally accepted that surface codes offer a promising way for achieving large-scale fault-tolerant quantum computation, partly because the syndrome measurements are based on nearest-neighbor interactions [45,46]. The syndrome measurements can be performed by acting Hadamard and CNOT gates in sequence on measurement and data qubits, followed by certain measurements [45]. The initialization and quantum operations on surface codes depend on established syndrome measurements aided by desired quantum operations acting on computational qubits [46]. Given the universal set of protected quantum gates explored in our scheme, both the initialization and quantum operations on surface codes can be preserved by geometry and holonomy, DFS and DD. Moreover, the protected quantum gates are executable in superconducting systems or trapped ions, and so it is possible to implement protected surface codes experimentally.

VI. CONCLUSIONS

To summarize, we present a scheme to achieve protected quantum operations in a hybrid manner, integrating geometry and holonomy, DD and dephasing-free features. Our scheme is based on one simple and well-developed interaction model, and in the scheme only two physical qubits are needed for encoding one computational qubit in favor of the noise-resistant approaches, and thus our scheme requires comparably less resource of qubits than that in the known schemes [27–30]. Due to the noise-resistant properties of the above mentioned approaches, the protected quantum operations are less sensitive to errors and therefore our scheme is essential in achieving noise-resistant quantum computation. We explore the implementation of the protected quantum operations in a superconducting system, in which adjustable QRM-QRM interaction between a neighbor pair is possible. Two desired effective Hamiltonians can be derived with only one or two external drivings for coupling two QRMs or two pairs of three QRMs, reducing the need for more resource and hence alleviating the scaling problem with external drivings. The set of hybridly protected quantum gates are useful in implementing various quantum-computation tasks due to their universality and robustness. Specifically, we discuss the implementation of surface codes on the basis of the protected quantum operations. Since our scheme mitigates errors in system evolution, the errors suffered at the level of creating QECCs and implementing quantum operations on QECCs can be reduced, and thus the opportunity of successfully executing QECCs can be enhanced. Our scheme is also workable in other superconducting systems since our desired interaction model has been experimentally achieved in Refs. [32–37]. Moreover, it has not escaped our notice that our scheme can be executed in a physical system of trapped ions [38–40], as well. The full connectivity of trapped ions makes the protected quantum operations even useful in achieving different robust quantum-computation tasks. Our scheme is

then scalable since it relies on the special form of system interaction, which can be achievable between different pairs of physical qubits. Therefore, our scheme brings us closer towards realizing protected quantum operations and so fault-tolerant quantum computation with near-term quantum devices since it is based on an experimentally achievable Hamiltonian.

ACKNOWLEDGMENTS

C.S. is supported by Fundamental Research Funds for the Central Universities (Grant No. 2412019FZ040). G.W. is supported by Fundamental Research Funds for the Central Universities (Grant No. 2412020FZ026) and Natural Science Foundation of Jilin Province (Grant No. JJKH20190279KJ). X. X.Y. is supported by National Natural Science Foundation of China (Grant No. 12175033).

APPENDIX A: GEOMETRIC FEATURE OF THE PROTECTED GATES

1. Geometric feature of $U_{2,1}(\tau_2)$

To show $U_{2,1}(\tau_2)$ is a geometric-phase gate, we explore the evolution of state $|1\rangle_A|1\rangle_L$ with the action of H_1 and H_2 in special sequence when the auxiliary qubit is in its ground state $|1\rangle_A$,

$$\begin{aligned}|1\rangle_A|1\rangle_L &\xrightarrow{e^{-i\pi/(4\Omega_{12})H_2}} |1\rangle_A|\alpha_m\rangle_L \xrightarrow{U_1(\tau_1)\big|_{\theta=0}} -|1\rangle_A|\alpha_p\rangle_L \\ &\xrightarrow{U_1(\tau_1)} e^{i\theta}|1\rangle_A|\alpha_m\rangle \xrightarrow{e^{i\pi/(4\Omega_{12})H_2}} e^{i\theta}|1\rangle_A|1\rangle_L,\end{aligned} \tag{A1}$$

where $|\alpha_m\rangle_L = (1/\sqrt{2})(|1\rangle_L - i|0\rangle_L)$ and $|\alpha_p\rangle_L = (1/\sqrt{2})(|1\rangle_L + i|0\rangle_L)$. The results show that θ is the total phase accumulated by the initial state from a cyclic evolution. During the evolution, there is no dynamic phase collected within θ since the parallel transport condition is fulfilled as shown in the following:

$$\begin{aligned}&\langle\psi(t)|H_2|\psi(t)\rangle = 0, \quad 0 \le t \le \tau_0,\\ &\langle\psi(t)|(H_1|_{\theta=0})|\psi(t)\rangle = 0, \quad \tau_0 \le t \le \tau_0+\tau_1,\\ &\langle\psi(t)|H_1|\psi(t)\rangle = 0, \quad \tau_0+\tau_1 \le t \le \tau_0+2\tau_1,\\ &\langle\psi(t)|H_2|\psi(t)\rangle = 0, \quad \tau_0+2\tau_1 \le t \le 2\tau_0+2\tau_1,\end{aligned} \tag{A2}$$

where $\tau_0 = (\pi/4\Omega_{12})$, $|\psi(t)\rangle = \tilde{U}(t)|1\rangle_A|1\rangle_L$ and $\tilde{U}(t)$ is given by

$$\tilde{U}(t) = \begin{cases} e^{-iH_2 t}, & 0 \le t \le \tau_0,\\ e^{-iH_1^0 t}e^{-iH_2\tau_0}, & \tau_0 \le t \le \tau_0+\tau_1,\\ e^{-iH_1 t}e^{-iH_1^0\tau_1}e^{-iH_2\tau_0}, & \tau_0+\tau_1 \le t \le \tau_0+2\tau_1,\\ e^{iH_2 t}e^{-iH_1\tau_1}e^{-iH_1^0\tau_1}e^{-iH_2\tau_0}, & \tau_0+2\tau_1 \le t \le 2\tau_0+2\tau_1,\end{cases} \tag{A3}$$

where $H_1^0 = H_1|_{\theta=0}$. In other words, θ is just a geometric phase without any dynamic phase accumulated during the evolution and hence, $U_{2,1}(\tau_2) = e^{-i\theta\sigma_z^L}$ expresses nothing but geometric-phase gates given different values of θ.

2. Two-qubit gate $U_3(\tau_1')$ and its geometric feature

Consider two computational qubits in the DFS of dephasing $\{|00\rangle_L, |01\rangle_L, |10\rangle_L, |11\rangle_L\}$ where $|00\rangle_L = |0\rangle_1|1\rangle_2|0\rangle_3|1\rangle_4$, $|01\rangle_L = |0\rangle_1|1\rangle_2|1\rangle_3|0\rangle_4$, $|10\rangle_L = |1\rangle_1|0\rangle_2|0\rangle_3|1\rangle_4$, and $|11\rangle_L = |1\rangle_1|0\rangle_2|1\rangle_3|0\rangle_4$. Control parameters of the system to get H_3, and we have an evolution operator from H_3,

$$U_3(\tau_1') = \begin{pmatrix} \cos\theta & -\sin\theta & 0 & 0\\ -\sin\theta & -\cos\theta & 0 & 0\\ 0 & 0 & -\cos\theta & -\sin\theta\\ 0 & 0 & -\sin\theta & \cos\theta\end{pmatrix} \tag{A4}$$

written in the basis of $\{|00\rangle_L, |01\rangle_L, |10\rangle_L, |11\rangle_L\}$.

It is not difficult to show that $U_3(\tau_1')$ illustrates geometric two-qubit gates. To achieve this, we recast $U_3(\tau_1')$ as

$$U_3(\tau_1') = U_{3,1}(\tau_1') \oplus U_{3,2}(\tau_1'), \tag{A5}$$

where $U_{3,m}(\tau_1') = (-1)^{m+1}\cos\theta\sigma_z^L - \sin\theta\sigma_x^L$. Define two subspaces $\mathcal{S}_0' = \{|00\rangle_L, |01\rangle_L\}$ and $\mathcal{S}_1' = \{|10\rangle_L, |11\rangle_L\}$ with the projection operators $P_{\mathcal{S}_0'} = |00\rangle_L\langle 00| + |01\rangle_L\langle 01|$ and $P_{\mathcal{S}_1'} = |10\rangle_L\langle 10| + |11\rangle_L\langle 11|$, respectively. We observe that $\mathcal{S}_m'(\tau_1') = U_3(\tau_1')\mathcal{S}_m' = \mathcal{S}_m'$ and $P_{\mathcal{S}_m'}(t)H_3P_{\mathcal{S}_m'}(t) = 0$, where $P_{\mathcal{S}_m'}(t) = U_3(t)P_{\mathcal{S}_m'}U_3^\dagger(t)$. We thus know that $U_{3,m}(\tau_1')$ are two holonomic matrices in the corresponding subspaces. As a result, $U_3(\tau_1')$ possesses the robust merit offered by the geometric feature.

It is worth mentioning that by considering the subspace $\mathcal{S}' = \{|00\rangle_L, |01\rangle_L, |10\rangle_L, |11\rangle_L\}$ with the corresponding projection $P_{\mathcal{S}'} = |00\rangle_L\langle 00| + |01\rangle_L\langle 01| + |10\rangle_L\langle 10| + |11\rangle_L\langle 11|$, we can also demonstrate the holonomic feature

of $U_3(\tau_1')$. Through calculations, we find $\mathcal{S}'(\tau_1') = U_3(\tau_1')\mathcal{S}' = \mathcal{S}'$ and $P_{\mathcal{S}'}(t)H_3P_{\mathcal{S}'}(t) = 0$, where $P_{\mathcal{S}'}(t) = U_3(t)P_{\mathcal{S}'}U_3^\dagger(t)$. So as a whole, $U_3(\tau_1')$ represents holonomic quantum gates acting on the subspace $\mathcal{S}'$.

3. Geometric feature of $U_4(\tau_2')$

$U_4(\tau_2')$ can be shown to be a geometric-phase gate in a similar way, investigating the evolution of state $|1\rangle_L|1\rangle_L$ with well-arranged Hamiltonians H_3 and H_4 in succession,

$$\begin{aligned}|1\rangle_L|1\rangle_L &\xrightarrow{e^{-i\pi/(4\Omega_{34})H_4}} |1\rangle_L|\alpha_m\rangle_L \xrightarrow{U_3(\tau_1')\big|_{\theta'=0}} |1\rangle_L|\alpha_p\rangle_L \\ &\xrightarrow{U_3(\tau_1')} e^{-i\theta'}|1\rangle_L|\alpha_m\rangle_L \xrightarrow{e^{i\pi/(4\Omega_{34})H_4}} e^{-i\theta'}|1\rangle_L|1\rangle_L. \quad \text{(A6)}\end{aligned}$$

θ' is the total phase gathered by the state $|1\rangle_L|1\rangle_L$ during the above explained cyclic evolution. Within θ', there is no contribution due to dynamic phase according to the parallel transport condition as illustrated,

$$\begin{aligned}&\langle\Psi(t)|H_4|\Psi(t)\rangle = 0, \quad 0 \le t \le \tau_0', \\ &\langle\Psi(t)|(H_3|_{\theta'=0})|\Psi(t)\rangle = 0, \quad \tau_0' \le t \le \tau_0' + \tau_1', \\ &\langle\Psi(t)|H_3|\Psi(t)\rangle = 0, \quad \tau_0' + \tau_1' \le t \le \tau_0' + 2\tau_1', \\ &\langle\Psi(t)|H_4|\Psi(t)\rangle = 0, \quad \tau_0' + 2\tau_1' \le t \le 2\tau_0' + 2\tau_1',\end{aligned} \quad \text{(A7)}$$

where $\tau_0' = (\pi/4\Omega_{34})$, $|\Psi(t)\rangle = \bar{U}(t)|1\rangle_L|1\rangle_L$ and $\bar{U}(t)$ is specified in the following:

$$\bar{U}(t) = \begin{cases} e^{-iH_4t}, & 0 \le t \le \tau_0', \\ e^{-iH_3^0t}e^{-iH_4\tau_0'}, & \tau_0' \le t \le \tau_0' + \tau_1', \\ e^{-iH_3t}e^{-iH_3^0\tau_1'}e^{-iH_4\tau_0'}, & \tau_0' + \tau_1' \le t \le \tau_0' + 2\tau_1', \\ e^{iH_4t}e^{-iH_3\tau_1'}e^{-iH_3^0\tau_1'}e^{-iH_4\tau_0'}, & \tau_0' + 2\tau_1' \le t \le 2\tau_0' + 2\tau_1', \end{cases} \quad \text{(A8)}$$

where $H_3^0 = H_3|_{\theta'=0}$. It is clearly demonstrated that θ' is purely geometric since no dynamic phase is piled up during the evolution and hence, $U_4(\tau_2') = e^{-i\theta'\sigma_z^L\otimes\sigma_z^L}$ describes geometric-phase gates dependent on the values of θ'.

APPENDIX B: DESIRED EFFECTIVE HAMILTONIANS IN COUPLED QRMS

We discuss the realization of the desired effective Hamiltonians in a superconducting system of coupled QRMs. As shown in Fig. 1, the system consists of an array of QRMs and each QRM is just one effective qubit. The coupling between QRMs is achieved by controllable hopping interaction via SQUID [43]. The system Hamiltonian of three-neighbor QRMs is given in Eq. (9). In the polariton basis of QRM, we can rewrite H_m^r $(m = 1, 2, 3)$ as $H_m^r = \sum_{\tilde{l}_m}\omega_{\tilde{l}_m}|\tilde{l}_m\rangle\langle\tilde{l}_m|$, where $|\tilde{l}_m\rangle$ represents the polariton basis of mth QRM. In the interaction picture with respect to $H_1^r + H_2^r + H_3^r$, we obtain the following interaction in the polariton basis of the QRMs [43]:

$$\begin{aligned}H_{c\mathrm{QRM}}^I = {} & J_{12}\cos(\omega_{12}t + \phi_{12})\Big(\sum_{\tilde{l}_1,\tilde{k}_1} c_{\tilde{l}_1\tilde{k}_1}|\tilde{l}_1\rangle\langle\tilde{k}_1|e^{-i\omega_{\tilde{k}_1\tilde{l}_1}t}\Big) \\ & \otimes\Big(\sum_{\tilde{l}_2,\tilde{k}_2} c_{\tilde{l}_2\tilde{k}_2}|\tilde{l}_2\rangle\langle\tilde{k}_2|e^{-i\omega_{\tilde{k}_2\tilde{l}_2}t}\Big) \\ & + J_{13}\cos(\omega_{13}t + \phi_{13})\Big(\sum_{\tilde{l}_1,\tilde{k}_1} c_{\tilde{l}_1\tilde{k}_1}|\tilde{l}_1\rangle\langle\tilde{k}_1|e^{-i\omega_{\tilde{k}_1\tilde{l}_1}t}\Big) \\ & \otimes\Big(\sum_{\tilde{l}_3,\tilde{k}_3} c_{\tilde{l}_3\tilde{k}_3}|\tilde{l}_3\rangle\langle\tilde{k}_3|e^{-i\omega_{\tilde{k}_3\tilde{l}_3}t}\Big),\end{aligned} \quad \text{(B1)}$$

where $c_{\tilde{l}_m\tilde{k}_m} = \langle\tilde{l}_m|((a_m^\dagger + a_m)|\tilde{k}_m\rangle$, and $\omega_{\tilde{k}_m\tilde{l}_m} = \omega_{\tilde{k}_m} - \omega_{\tilde{l}_m}$.

When higher levels can be neglected by adjusting system parameters, we consider only the two lowest levels $\tilde{0}$ and $\tilde{1}$ and obtain

$$\begin{aligned}H_{c\mathrm{QRM}}^{rI} = {} & J_{12}\cos(\omega_{12}t + \phi_{12})\big(c_{\tilde{0}_1\tilde{1}_1}|\tilde{0}_1\rangle\langle\tilde{1}_1|e^{-i\omega_{\tilde{1}_1\tilde{0}_1}t} + \mathrm{h.c.}\big) \\ & \otimes\big(c_{\tilde{0}_2\tilde{1}_2}|\tilde{0}_2\rangle\langle\tilde{1}_2|e^{-i\omega_{\tilde{1}_2\tilde{0}_2}t} + \mathrm{h.c.}\big) \\ & + J_{13}\cos(\omega_{13}t + \phi_{13}) \\ & \times\big(c_{\tilde{0}_1\tilde{1}_1}|\tilde{0}_1\rangle\langle\tilde{1}_1|e^{-i\omega_{\tilde{1}_1\tilde{0}_1}t} + \mathrm{h.c.}\big) \\ & \otimes\big(c_{\tilde{0}_3\tilde{1}_3}|\tilde{0}_3\rangle\langle\tilde{1}_3|e^{-i\omega_{\tilde{1}_3\tilde{0}_3}t} + \mathrm{h.c.}\big).\end{aligned} \quad \text{(B2)}$$

Assuming $|J_{mn}c_{\tilde{0}_m\tilde{1}_m}c_{\tilde{0}_n\tilde{1}_n}| \ll \omega_{\tilde{1}_m\tilde{0}_m} + \omega_{\tilde{1}_n\tilde{0}_n} \pm \omega_{mn}$, and $\omega_{mn} = \omega_{\tilde{1}_n\tilde{0}_n} - \omega_{\tilde{1}_m\tilde{0}_m}$, we obtain an effective interaction Hamiltonian according to the rotating-wave approximation,

$$H_{c\mathrm{QRM}}^{\mathrm{eff}} = \Omega_{12}\left(\tilde{\sigma}_+^1\tilde{\sigma}_-^2 + \tilde{\sigma}_-^1\tilde{\sigma}_+^2\right) + \Omega_{13}\left(\tilde{\sigma}_+^1\tilde{\sigma}_-^3 + \tilde{\sigma}_-^1\tilde{\sigma}_+^3\right), \quad \text{(B3)}$$

where $\Omega_{mn} = J_{mn} c_{\tilde{0}_m \tilde{1}_m} c_{\tilde{0}_n \tilde{1}_n}/2$ and $\phi_{mn} = 0$, $\tilde{\sigma}_+^m = |\tilde{0}_m\rangle\langle\tilde{1}_m|$ and $\tilde{\sigma}_-^m = |\tilde{1}_m\rangle\langle\tilde{0}_m|$ represent the Pauli operations acting on effective qubits. It is easy to find that the coupling strength Ω_{mn} can be negative when choosing $\phi_{mn} = \pi$.

The $H_{c\mathrm{QRM}}^{\mathrm{eff}}$ is nothing but Eq. (1) with $\tilde{\sigma}_\pm^m$ replaced by $\sigma_\pm^m$ [43]. Therefore, H_1 and H_3 are implementable in the coupled QRMs by adjusting the interactions among QRMs. In the case that H_2 or H_4 is needed, we keep only the coupling strength between QRMs 2 and 3, or 3 and 4 via controlling SQUID devices. It is clearly shown in the effective Hamiltonian (B3) that the two desired effective Hamiltonians for realizing different protected single- and two-qubit quantum gates can be derived with only one (for interacting two QRMs) or two (for interacting two pairs of three QRMs) external drivings that are under control, reducing the need for more resource of external drivings.

We perform numerical calculations to check the validity of the approximation utilized in deriving $H_{c\mathrm{QRM}}^{\mathrm{eff}}$. We randomly choose 30 initial states of the form $|\phi_0\rangle = \sum_{u,v,w=0,1} a_{uvw} |\tilde{u}\tilde{v}\tilde{w}\rangle$, where $|\tilde{u}\tilde{v}\tilde{w}\rangle = |\tilde{u}_1\rangle|\tilde{v}_2\rangle|\tilde{w}_3\rangle$, and calculate the fidelities defined by

$$
\begin{aligned}
F^{(2)} &= \left| \langle\phi_0| e^{i\int_0^T H_{c\mathrm{QRM}}^{rI} dt} e^{-i\int_0^T H_{c\mathrm{QRM}}^{\mathrm{eff}} dt} |\phi_0\rangle \right|^2, \\
F^{(n)} &= \left| \langle\phi_0| e^{i\int_0^T H_{c\mathrm{QRM}}^{I} dt} e^{-i\int_0^T H_{c\mathrm{QRM}}^{\mathrm{eff}} dt} |\phi_0\rangle \right|^2,
\end{aligned}
\tag{B4}
$$

where $T = \pi/\Omega$ with $\Omega = \sqrt{\Omega_{12}^2 + \Omega_{13}^2}$, and the superscript $^{(n)}$ indicates the number of lowest energy levels considered in the calculations. Apparently, $F^{(2)}$ tells us how close is $H_{c\mathrm{QRM}}^{rI}$ to the effective Hamiltonian, and $F^{(n)}$ indicates how well is the effective Hamiltonian approximated by $H_{c\mathrm{QRM}}^{I}$. Since there are so many energy levels included in $H_{c\mathrm{QRM}}^{I}$, it is reasonable to select some of the lowest levels in numerical simulations, and we choose the lowest three, five, and seven levels, respectively. The system parameters are selected as $\omega_m^c = 2\pi \times 7$ GHz, $\omega_1^q = 2\pi \times 6.1$ GHz, $\omega_2^q = \omega_3^q = 2\pi \times 5.1$ GHz $g_m = 2\pi \times 2$ GHz, $\phi_{12} = \phi_{13} = 0$, $J_{12} = 2\sin(\theta/2)\Omega/(c_{\tilde{0}_1\tilde{1}_1} c_{\tilde{0}_2\tilde{1}_2})$, and $J_{13} = 2\cos(\theta/2)\Omega/(c_{\tilde{0}_1\tilde{1}_1} c_{\tilde{0}_3\tilde{1}_3})$ where $\Omega = 2\pi \times 2$ MHz, $\theta = -\pi/4$ and photon number $n = 20$ or 30. The results are summarized in Figs. 2(a) and 2(b), showing $F^{(2)}, F^{(3)}, F^{(5)}$, and $F^{(7)}$ versus evolution time t when $n = 20$ or 30. The two subfigures show clearly that $n = 20$ is large enough for obtaining excellent approximation since the numerical results from $n = 20$ and $n = 30$ are extremely near to each other. In either subfigure, the four curves representing $F^{(n)}$ are indeed very close to 1, and the more the energy levels, the worse the fidelities are. Specifically, $F^{(5)}$ and $F^{(7)}$ almost overlap, and the results demonstrate that higher-energy levels can be neglected effectively based on the properly selected system parameters. We thus explore the fidelities of different protected gates by including two lowest levels when $n = 20$ in Tables I, II, and III. Moreover, in comparing different $F^{(n)}$, we choose $|\phi_0\rangle$ as initial states, in which all eight-state $|\tilde{u}\tilde{v}\tilde{w}\rangle$ may be included dependent on coefficients a_{uvw}. While when we calculate gate fidelities, we focus only on certain subspaces by encoding effective qubits to obtain computational qubits. It is therefore possible that higher gate fidelities than $F^{(n)}$ can be obtained.

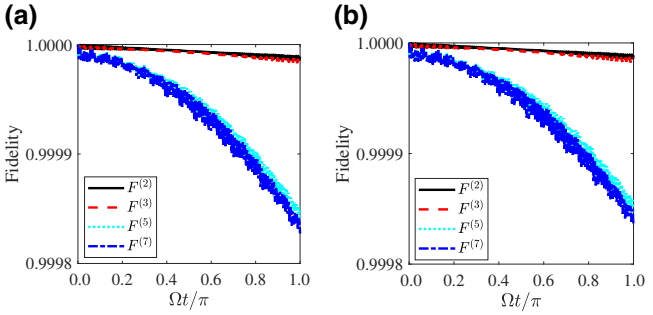

FIG. 2. Numerical results showing the validity of the approximation utilized in deriving $H_{c\mathrm{QRM}}^{\mathrm{eff}}$, (a) is obtained when photon number is $n = 20$, and (b) is for $n = 30$.

APPENDIX C: PROTECTION FROM DECOHERENCES BY THE PDD PULSE SEQUENCES

With the system-environment coupling, we write the total Hamiltonian of system and environment as $H_T = H_s + H_B + H_{SB}$, where H_s is the system Hamiltonian, H_B is the Hamiltonian of environment and H_{SB} describes the system-environment interaction. Follow Ref. [18], we choose

$$
H_B = J_B \sum_{m<n}^{N} (\tilde{\sigma}_y^m \tilde{\sigma}_y^n + \tilde{\sigma}_z^m \tilde{\sigma}_z^n - 2\tilde{\sigma}_x^m \tilde{\sigma}_x^n)/|m-n|^3, \tag{C1}
$$

and

$$
H_{SB} = B_0 \sum_{\nu=x,y,z} \sum_{m=1}^{N} \tilde{\sigma}_\nu^m \otimes B_\nu^m, \tag{C2}
$$

where $B_\nu^m = \sum_{n=1}^{N} \tilde{\sigma}_\nu^n / 2^{|m-n|}$, and $N = 3$ or 4 for single- or two-qubit gates. In our calculations with coupled QRMs, H_s is the system Hamiltonian (B2) with controllable parameters, and the Pauli operators in H_B and H_{SB} are the ones acting on effective qubits. We here utilize the commonly used DD technique, PDD, which employs repeated base pulse sequence of $Z[\cdot]X[\cdot]Z[\cdot]X[\cdot]$ to approximately average decoherences out and specifically, $Z = \tilde{\sigma}_z^{\otimes N}$ and $X = \tilde{\sigma}_x^{\otimes N}$. When taking H_B and H_{SB} into numerical calculations, the dimension of the total Hamiltonian H_T is very large and it is difficult to numerically manage the calculations of the large dimension. As a result, we choose

only two lowest energy levels of each QRM to reduce the difficulty encountered in numerical calculations. We select $10B_0 = J_B = \Omega = \Omega'$ and repeat the base pulse sequence 10 times to obtain the gate fidelities in the presence of decoherences, as shown in Table III. It is clearly shown in the table that the PDD preferably protects the quantum gates from the decoherences happened in all x, y, and z directions. Further improved gate fidelities are attainable if we increase the number of times of repeating the base pulse sequence. Since the desired effective Hamiltonians commute with the decoupling group, any DD technique utilizing the pulses formed by the decoupling group elements is workable in our scheme to fight against decoherences.

We explore the gate performance in the presence of the system-environment interaction in x, y, and z directions. The environmental noises generally cause fluctuations in effective qubits or QRMs, written in terms of $\delta_x\tilde{\sigma}_x$, $\delta_y\tilde{\sigma}_y$, and $\delta_z\tilde{\sigma}_z$. The DD technique protects quantum operations against all the single-effective-qubit errors according to its working principle, as reflected in our numerical results. Particularly, in the superconducting system, the fluctuations in effective qubits may be caused by different environmental noises such as field noise, charge noise, or resonator noise, etc. The DD technique is helpful in fighting against these errors.

[1] D. P. DiVincenzo and P. W. Shor, Fault-Tolerant Error Correction with Efficient Quantum Codes, Phys. Rev. Lett. **77**, 3260 (1996).

[2] M. A. Nielsen and I. L. Chuang, *Quantum Computation and Quantum Information* (Cambridge University Press, New York, 2000).

[3] E. Knill, Quantum computing with realistically noisy devices, Nature **434**, 39 (2005).

[4] D. Aharonov and M. Ben-Or, in *Proc. 29th Ann. ACM Symp. on Theory of Computing*, 176 (ACM Press, New York, 1997).

[5] A. Y. Kitaev, Quantum computations: Algorithms and error correction, Russian Math. Surveys **52**, 1191 (1997).

[6] E. Knill, R. Laflamme, and W. H. Zurek, Resilient quantum computation: Error models and thresholds, Proc. Roy. Soc. A **454**, 365 (1998).

[7] S. Endo, S. C. Benjamin, and Y. Li, Practical Quantum Error Mitigation for Near-Future Application, Phys. Rev. X **8**, 031027 (2018).

[8] S. Zhang, Y. Lu, K. Zhang, W. Chen, Y. Li, J.-N. Zhang, and K. Kim, Error-mitigated quantum gates exceeding physical fidelities in a trapped-ion system, Nat. Commun. **11**, 587 (2020).

[9] M. V. Berry, Quantal phase factors accompanying adiabatic changes, Proc. R. Soc. A **392**, 45 (1984).

[10] Y. Aharonov and J. Anandan, Phase Change during a Cyclic Quantum Evolution, Phys. Rev. Lett. **58**, 1593 (1987).

[11] P. Zanardi and M. Rasetti, Holonomic quantum computation, Phys. Lett. A **264**, 94 (1999).

[12] E. Sjöqvist, D. M. Tong, L. M. Andersson, B. Hessmo1, M. Johansson, and K. Singh, Non-adiabatic holonomic quantum computation, New J. Phys. **14**, 103035 (2012).

[13] V. A. Mousolou, C. M. Canali, and E. Sjöqvist, Universal non-adiabatic holonomic gates in quantum dots and single-molecule magnets, New J. Phys. **16**, 013029 (2014).

[14] P. Z. Zhao, X.-D. Cui, G. F. Xu, E. Sjöqvist, and D. M. Tong, Rydberg-atom-based scheme of nonadiabatic geometric quantum computation, Phys. Rev. A **96**, 052316 (2017).

[15] L. Viola, E. Knill, and S. Lloyd, Dynamical Decoupling of Open Quantum Systems, Phys. Rev. Lett. **82**, 2417 (1999).

[16] D. Li, A. E. Dementyev, Y. Q. Dong, R. G. Ramos, and S. E. Barrett, Generating Unexpected Spin Echoes in Dipolar Solids with π Pulses, Phys. Rev. Lett. **98**, 190401 (2007).

[17] J. J. L. Morton, A. M. Tyryshkin, R. M. Brown, S. Shankar, B. W. Lovett, A. Ardavan, T. Schenkel, E. E. Haller, J. W. Ager, and S. A. Lyon, Solid-state quantum memory using the 31P nuclear spin, Nature **455**, 1085 (2008).

[18] J. R. West, D. A. Lidar, B. H. Fong, and M. F. Gyure, High Fidelity Quantum Gates via Dynamical Decoupling, Phys. Rev. Lett. **105**, 230503 (2010).

[19] L.-M. Duan and G.-C. Guo, Preserving Coherence in Quantum Computation by Pairing Quantum Bits, Phys. Rev. Lett. **79**, 1953 (1997).

[20] P. Zanardi and M. Rasetti, Noiseless Quantum Codes, Phys. Rev. Lett. **79**, 3306 (1997).

[21] D. A. Lidar, I. L. Chuang, and K. B. Whaley, Decoherence-Free Subspaces for Quantum Computation, Phys. Rev. Lett. **81**, 2594 (1998).

[22] O. Oreshkov, T. A. Brun, and D. A. Lidar, Fault-Tolerant Holonomic Quantum Computation, Phys. Rev. Lett. **102**, 070502 (2009).

[23] O. Oreshkov, T. A. Brun, and D. A. Lidar, Scheme for fault-tolerant holonomic computation on stabilizer codes, Phys. Rev. A **80**, 022325 (2009).

[24] Y.-C. Zheng and T. A. Brun, Fault-tolerant holonomic quantum computation in surface codes, Phys. Rev. A **91**, 022302 (2015).

[25] J. Zhang, S. J. Devitt, J. Q. You, and F. Nori, Holonomic surface codes for fault-tolerant quantum computation, Phys. Rev. A **97**, 022335 (2018).

[26] C. Wu, Y. Wang, X.-L. Feng, and J.-L. Chen, Holonomic Quantum Computation in Surface Codes, Phys. Rev. Appl. **13**, 014055 (2020).

[27] G. F. Xu, J. Zhang, D. M. Tong, E. Sjöqvist, and L. C. Kwek, Nonadiabatic Holonomic Quantum Computation in Decoherence-Free Subspaces, Phys. Rev. Lett. **109**, 170501 (2012).

[28] G. F. Xu and G. L. Long, Protecting geometric gates by dynamical decoupling, Phys. Rev. A **90**, 022323 (2014).

[29] Z.-Y. Xue, J. Zhou, and Z. D. Wang, Universal holonomic quantum gates in decoherence-free subspace on superconducting circuits, Phys. Rev. A **92**, 022320 (2015).

[30] X. Wu and P. Z. Zhao, Universal nonadiabatic geometric gates protected by dynamical decoupling, Phys. Rev. A **102**, 032627 (2020).

[31] C. Sun, G. Wang, C. Wu, H. D. Liu, X. L. Feng, J. L. Chen, and K. Xue, Non-adiabatic holonomic quantum

computation in linear system-bath coupling, Sci. Rep. **6**, 20292 (2016).
[32] J. Q. You, J. S. Tsai, and F. Nori, Scalable Quantum Computing with Josephson Charge Qubits, Phys. Rev. Lett. **89**, 197902 (2002).
[33] A. O. Niskanen, K. Harrabi, F. Yoshihara, Y. Nakamura, S. Lloyd, and J. S. Tsai, Quantum coherent tunable coupling of superconducting qubits, Science **316**, 723 (2007).
[34] J. Majer, J. M. Chow, J. M. Gambetta, Jens Koch, B. R. Johnson, J. A. Schreier, L. Frunzio, D. I. Schuster, A. A. Houck, A. Wallraff, A. Blais, M. H. Devoret, S. M. Girvin, and R. J. Schoelkopf, Coupling superconducting qubits via a cavity bus, Nature **449**, 443 (2007).
[35] M. Reagor *et al.*, Demonstration of universal parametric entangling gates on a multi-qubit lattice, Sci. Adv. **4**, eaao3603 (2018).
[36] D. M. Abrams, N. Didier, B. R. Johnson, M. P. da Silva, and C. A. Ryan, Implementation of the XY interaction family with calibration of a single pulse abrams, Nat. Electron. **3**, 744 (2020).
[37] X. Li, T. Cai, H. Yan, Z. Wang, X. Pan, Y. Ma, W. Cai, J. Han, Z. Hua, X. Han, Y. Wu, H. Zhang, H. Wang, Y. Song, L. Duan, and L. Sun, Tunable Coupler for Realizing a Controlled-Phase Gate with Dynamically Decoupled Regime in a Superconducting Circuit, Phys. Rev. Appl. **14**, 024070 (2020).
[38] K. Mølmer and A. Sørensen, Multiparticle Entanglement of Hot Trapped Ionss, Phys. Rev. Lett. **82**, 1835 (1999).
[39] C. A. Sackett, D. Kielpinski, B. E. King, C. Langer, V. Meyer, C. J. Myatt, M. Rowe, Q. A. Turchette, W. M. Itano, D. J. Wineland, and C. Monroe, Experimental entanglement of four particles, Nature **404**, 256 (2000).
[40] J. Benhelm, G. Kirchmair, C. F. Roos, and R. Blatt, Towards fault-tolerant quantum computing with trapped ions, Nat. Phys. **4**, 463 (2008).
[41] L. Viola, S. Lloyd, and E. Knill, Universal Control of Decoupled Quantum Systems, Phys. Rev. Lett. **83**, 4888 (1999).
[42] P. Zanardi, Stabilizing quantum information, Phys. Rev. A **63**, 012301 (2000).
[43] Y. Wang, Y. Su, X. Chen, and C. Wu, Dephasing-Protected Scalable Holonomic Quantum Computation on a Rabi Lattice, Phys. Rev. Appl. **14**, 044043 (2020).
[44] R. Stassi1 and F. Nori, Long-lasting quantum memories: Extending the coherence time of superconducting artificial atoms in the ultrastrong-coupling regime, Phys. Rev. A **97**, 033823 (2018).
[45] A. G. Fowler, M. Mariantoni, J. M. Martinis, and A. N. Cleland, Surface codes: Towards practical large-scale quantum computation, Phys. Rev. A **86**, 032324 (2012).
[46] C. Horsman, A. G. Fowler, S. Devitt, and R. V. Meter, Surface code quantum computing by lattice surgery, New J. Phys. **14**, 123011 (2012).